



**HAL**  
open science

# Spectral Analysis of the Response of Coarse Granular Material to Dynamic Penetration Test Modelled with DEM

Quoc Anh Tran, Bastien Chevalier, Pierre Breul

► **To cite this version:**

Quoc Anh Tran, Bastien Chevalier, Pierre Breul. Spectral Analysis of the Response of Coarse Granular Material to Dynamic Penetration Test Modelled with DEM. *International Journal of Geosynthetics and Ground Engineering*, 2018, 4, pp.22. 10.1007/s40891-018-0139-5 . hal-01885925

**HAL Id: hal-01885925**

**<https://uca.hal.science/hal-01885925>**

Submitted on 17 Nov 2020

**HAL** is a multi-disciplinary open access archive for the deposit and dissemination of scientific research documents, whether they are published or not. The documents may come from teaching and research institutions in France or abroad, or from public or private research centers.

L'archive ouverte pluridisciplinaire **HAL**, est destinée au dépôt et à la diffusion de documents scientifiques de niveau recherche, publiés ou non, émanant des établissements d'enseignement et de recherche français ou étrangers, des laboratoires publics ou privés.

1 Spectral analysis of the response of coarse granular material  
2 to dynamic penetration test modelled with DEM  
3

4 Quoc Anh Tran, Bastien Chevalier and Pierre Breul

5 Correspondence to [bastien.chevalier@uca.fr](mailto:bastien.chevalier@uca.fr)

6  
7 Université Clermont Auvergne, CNRS, SIGMA Clermont, Institut Pascal, F-63000  
8 CLERMONT-FERRAND, FRANCE

9 Tel. +33(0)4.73.40.75.23

10 Fax. +33(0)4.73.40.74.94  
11  
12  
13  
14  
15  
16  
17  
18  
19  
20  
21  
22

## 23 Abstract

24 Dynamic penetration tests are often used to determine the strength properties of surface soils.  
25 The paper presents a study on the use of spectral analysis on dynamic cone penetration tests  
26 results, modelled with Discrete Element Method. This method is applied to assess the effect of  
27 the variation of the grain size distribution of the soil on test results. A two-dimensional discrete  
28 model is used to reproduce cone penetration tests in dynamic conditions: the tip of the  
29 penetrometer is driven in the material by successive impacts of a hammer on the penetrometer.  
30 For each impact of the hammer, a curve of the load applied by the tip on the soil is obtained  
31 versus the penetration distance of the tip. The curves of the load vs. penetration traditionally  
32 used to calculate the tip resistance of the soil are analyzed with Discrete Fourier transform in  
33 order to investigate curve's shape. The effect of the variation of the grain size distribution of  
34 the soil on these curves is investigated, i.e. average particle diameter and span of particle size  
35 distribution. It was found out that the grain size distribution influences tip resistance but also  
36 the shape and oscillation modes of the curve of the stress-penetration curve. Based on these  
37 indicators, the exploitation of the load-displacement curve obtained with dynamic penetration  
38 tests could be enlarged to determine other properties of the soils.

39 Keywords: dynamic cone penetration, discrete element method, granular material, particle size  
40 distribution, Discrete Fourier Transform.

## 41 1. Introduction

42 In the practice of geotechnical engineering, the use of in situ testing is widespread. Among  
43 existing testing techniques, lightweight dynamic penetration testing device such as Panda  
44 penetrometer is used to characterize mechanical properties of surface soils [1,2]. Based on  
45 recent technological improvements, this device is able to record the curve of the tip stress or tip  
46 force versus the tip penetration distance for each impact of the hammer on the penetrometer  
47 [3,4]. This curve, referred to as load-penetration curve, provides information on dynamic tip  
48 resistance but also on additional mechanical parameters involved during the driving of the tip  
49 [3,5,6]. Cone penetration test is a blind testing technique, because there is no sampling of the  
50 different layers of soils that are cut across. It would be very interesting to be able to get  
51 information about the nature of the soils, from the actual measurements recorded by the device.  
52 The present paper proposes to study the effect of the particle size distribution on the load vs.  
53 penetration distance measured at the tip. Numerical modelling using Discrete Element Method

54 was chosen so that we have a strict control on the parameters of the particle size distribution  
55 (PSD).

56 The numerical model of penetration tests using Discrete Element Method (DEM) used to  
57 reproduce the penetration tests in dynamic conditions is the same model as the one presented  
58 in [7]. Many authors have modeled cone penetration tests before with DEM in 2D [8-15] and  
59 in 3D [3,16-20]. However, most of them modelled the penetration in static conditions, i.e. with  
60 a constant velocity of the tip, and very few focused on penetration tests in dynamic conditions,  
61 i.e. with impacts [6,7,19].

62 At the macroscopic scale, the tip resistance quantifies the mechanical response of the granular  
63 material to the driving of the tip (Fig.1). At the scale of the contacts or of the particles, the  
64 shapes of the load-penetration curves are analyzed in terms of both frequency and amplitude of  
65 signal oscillation by using Discrete Fourier Transform (DFT). Figure 2 shows an example of  
66 the load penetration curve. The objective of the study is to evaluate the effect of the PSD on the  
67 load-penetration curves, based on DFT analysis. Two parameters were tested: the average  
68 particle diameter,  $D_{50}$  and the span of the PSD given as the ratio of maximal particle diameter  
69  $D_{max}$  to minimal diameter  $D_{min}$ .

70 At first, we will present the numerical model and parameters used to reproduce the dynamic  
71 penetration test as well as the method used to analyze the load-penetration curve with DFT.  
72 Finally, the influence of the particle size distribution is discussed.

## 73 2. Numerical model

74 Discrete Element Method in two dimensions is used with Itasca software PFC<sup>2D</sup> [21]. Dense  
75 assemblies of disks are generated without gravity and without friction in a container of 0.60 m  
76 in width and of 0.45 m in height (Fig.3). The lateral walls of the container are fixed. A study of  
77 boundary conditions with different sample sizes on this numerical model was conducted by  
78 Tran et al. [14] and revealed that for a container width larger than 0.60 m, there is no effect of  
79 the lateral walls on the tip resistance anymore. A linear contact model is used along with a  
80 Coulomb friction criterion after the generation process. The normal contact stiffness of  
81  $1.25 \times 10^8$  N/m is chosen in order to assess the assumption of rigid particles during penetration  
82 tests [22-24]. The tangential contact stiffness has been set to 0.75 of normal contact stiffness.

83 The samples are generated without friction and without gravity in order to reach a random close  
84 packing volume fraction, corresponding to the minimal void ratio of the considered PSD. After

85 sample generation, gravity is applied to the system as well as a confining vertical stress of  
86 40 kPa. The confining stress is applied on the top face of the container to simulate an overlaying  
87 layer of material and to prevent the effects of free surface to be observed [1].

88 The penetration tests were performed with a frictionless rod of width  $D_{rod} = 14$  mm linked to a  
89 tip of width  $D_{tip} = 16$  mm at its bottom edge which has a friction coefficient  $\mu_{tip}$  of 0.3 [19]. First,  
90 the rod is driven with constant velocity until a depth of 0.15 m is reached inside the granular  
91 material. Then, the rod is released and stabilized under its own weight. Finally, series of five  
92 successive impacts are produced in the sample with a hammer represented by an additional disk  
93 hitting the top of the rod (Fig.3). The mass of the impacting cylinder is equal to the rod mass.  
94 The impacting velocity at the impact is equal to  $1,25 \text{ m}\cdot\text{s}^{-1}$  in order to obtain an average  
95 penetration distance that is representative of experimental tests. The description of the model  
96 and the effect of the impact velocity are addressed by Tran et al. in [7]. Table 1 summarizes the  
97 main parameters of the model.

98 Table 2 summarizes the parameters of the five granular materials studied, with two types of  
99 PSD. The first distribution type (I) keeps constant the ratio between maximal and minimal  
100 particle diameters  $D_{max}/D_{min} = 2$ , and particle number varies from 10 000 to 160 000 making  
101 the average diameter  $D_{50}$  varying (Fig.4 a). The second distribution type (II) keeps constant  
102 maximal diameter  $D_{max} = 7.02$  mm and the ratio between maximal and minimal particle  
103 diameters  $D_{max}/D_{min}$  varies from 2 to 10 (Fig.4 b). All the samples were tested with their  
104 maximal volume fraction ( $\phi_{max}$ ) and with a particle friction coefficient equal to 1.0.

105 For each type of granular material, the testing process was repeated on three different samples  
106 corresponding to the same sample conditions but with different initial particle arrangements.

107 The following section explains how the load-penetration curves obtained from dynamic cone  
108 penetration tests were analyzed in the frequency domain by using *DFT*.

### 109 3. Investigation of load - penetration curve

#### 110 3.1. Macroscopic exploitation for the tip resistance

111 Tip force  $F_d$  is defined as the vertical component of the force applied by the granular material  
112 on the tip as it drives in the granular with a penetration distance  $s$ . Figure 5 shows examples of  
113 load-penetration curves  $F_d = f(s)$  obtained for 3 impacts with the numerical model on the  
114 material *B*. The response obtained with the model is similar to the one classically obtained  
115 experimentally [4].

116 At the end of the driving process, the tip reaches a final position corresponding to a residual  
 117 penetration distance  $s_{res}$ . We can notice that there is a difference between the maximal  
 118 penetration distance  $s_{max}$  and the final residual penetration distance  $s_{res}$  (Fig.5). However, the  
 119 mechanical work of the tip force between these two positions is negligible due to the value of  
 120 the tip force between these two positions. Consequently, the dynamic tip resistance  $R_d$  of the  
 121 granular material for one impact was calculated as the average tip force  $F_d$  for penetration  
 122 distance between 0 and  $s_{max}$ :

$$R_d = \frac{1}{s_{max}} \int_{t=0}^{t_{s_{max}}} F_d(t) ds(t) \quad (1)$$

123 with:  $t$  the time;  $t_{s_{max}}$  the time when penetration distance is maximal and equal to  $s_{max}$ . Then,  
 124  $\langle R_d \rangle$  is the average value of dynamic tip resistances obtained for the five impacts and for the  
 125 three samples.

### 126 3.2. Frequency analysis using Discrete Fourier Transform

127 Each load-penetration curve presents variations - i.e. oscillations, peaks - observed between the  
 128 time of the impact and the time when the system stabilizes again (Fig.5). As the properties of  
 129 the granular material change, the shape and size of these variations change too. Consequently,  
 130 the load-penetration curve can provide not only the tip resistance of granular media but also  
 131 information on the granular material properties.

132 Fourier transformation provides a powerful way for study discrete data acquisition in the  
 133 frequency domain. It allows to decompose a signal into the frequencies that make it up. Discrete  
 134 Fourier Transform (DFT) changes the  $N$  "temporal" points  $y_n(x)$  in to  $N$  "frequency" points  $Y_k$   
 135 and inverse DFT the other way around by using the following equations:

$$Y_k = \sum_{n=0}^{N-1} y_n e^{-2\pi i n k / N}$$

$$y_n = \sum_{k=0}^{N-1} Y_k e^{2\pi i n k / N} \quad (2)$$

136 with:  $y_n$  the original function,  $Y_k$  the transformed function and  $N$ -points DFT.

137 The *DFT* bins ( $f_k$ ) represent frequencies in the discrete Fourier transform that are spaced at  
 138 intervals of  $\Delta f_k = F_s / N$ , where  $F_s$  is the sample rate equal to  $1/\Delta x$ , with  $\Delta x$  the recording interval.  
 139 All of load-penetration curve have been analyzed in frequency domain with  $F_s = 10^5 [m^{-1}]$  and  
 140 frequency resolution  $\Delta f_k = F_s / N = 0.1$ . The equation of inverse *DFT* can be computed by the  
 141 following formula:

$$y_n = \sum_{k=0}^{N-1} A_k \cos(2\pi f_k x + \varphi) \quad (3)$$

142 with:  $f_k$  the  $k^{th}$  frequency,  $A_k$  the associated amplitude and  $\varphi$  the phase of  $Y_k$  with

$$\varphi = \tan^{-1}(\text{Im}(Y_k)/\text{Re}(Y_k)) \quad (4)$$

143 In order to obtain a stabilized and accurate amplitude spectrum, it is necessary to ensure that  
 144 the number of DFT points is sufficient. Thus, the original signal of tip force versus penetration  
 145 distance is padded with trailing zeros to increase its length, before computing the DFT.

146 Figure 6 presents one example of the amplitude spectrum when the  $N$ -points of DFT is equal to  
 147 1, 4 and 16 times respectively the number of data of the signal detected between  $s = 0$  and  
 148  $s = s_{max}$  for one impact in the material  $A$ . We found that the amplitude spectrum becomes stable  
 149 when  $N$ -points DFT increases.

150 Figure 7 presents two examples of amplitude spectrum related to the materials  $A$  and  $C$   
 151 corresponding respectively to maximal and minimal average particle diameters. The first part  
 152 of the spectrum i.e.  $f_k < 100 [m^{-1}]$  corresponds to a transition zone where amplitude spectrum  
 153 decreases rapidly. Thus, we introduce one parameter called ( $f_{trans}$ ) which is the frequency  
 154 corresponding to the first local minimum value of the amplitude spectrum (Fig.6).

155 In order to analyze the oscillations of the load-penetration curves, we studied the range of  
 156 frequencies that provides the most significant information to rebuild the signal with inverse  
 157 DFT and to filter the signal noise. For that purpose, the relative error RE between the  
 158 reconstructed signal of the  $k$  first components ( $y_k$ ) based on Eq. 3 and the original signal ( $y$ )  
 159 described by the following equation has been computed.

$$RE = \frac{\sum_1^N \|y^i - y_{k=0:i}^i\| \times (x^i - x^{i-1})}{\sum_i^N y^i \times (x^i - x^{i-1})} \quad (5)$$

160 Figure 8 presents the relative error ( $RE$ ) for one impact of the material  $A$ . The range of  
 161 frequencies  $[0, f_{limit}]$  that gives an RE smaller than 10% was chosen for rebuilding the signal  
 162 and for the load-penetration curves analysis. Note that, the more RE decreases, the more the  
 163 reconstructed signal is accurate in comparison to the raw signal.

164 Figure 9 presents one example of signal reconstruction for the material  $A$ . We found that the  
 165 signal reconstructed with the frequency range  $[0, f_{trans}]$  provides the general trend (baseline) of  
 166 the load-penetration curve. The signal reconstructed with the frequency range  $[0, f_{limit}]$  provides  
 167 a reliable reconstruction of the raw signal without noise. Thus, we define the band-pass of

168 frequency (BF range) from  $f_{trans}$  to  $f_{limit}$ , for obtaining the full oscillation information of load-  
169 penetration curve. The reconstructed signal with  $[f_{trans}, f_{limit}]$  frequency range presents the major  
170 oscillations of load-penetration curve.

#### 171 4. Effect of PSD variation

172 The effect of PSD on the load-penetration curve in terms of tip resistance  $\langle R_d \rangle$  and in frequency  
173 domain by using the frequencies detected in band-pass range  $[f_{trans}, f_{limit}]$  is presented in this  
174 section. The PSD types I and II are studied in this section (Tab.2).

175 Figure 10 presents the load-penetration curves of 5 impacts for materials A, B and C. These  
176 materials have the same ratio  $D_{max}/D_{min} = 2$  and  $D_{50}$  of respectively 7.02 mm, 3.51 mm and  
177 1.76 mm. Figure 11 presents the load-penetration curves of 5 successive impacts for the  
178 materials A, D and E. These materials have a ratio  $D_{max}/D_{min}$  of respectively 2, 5 and 10, and  
179 the same maximal diameter  $D_{max}$  of 7.02 mm. We found that the final penetration distance and  
180 the signals oscillations amplitude increases as  $D_{50}$  decreases and  $D_{max}/D_{min}$  ratio increases.

181 Concerning the macroscopic response, Figure 12 shows  $\langle R_d \rangle$  as function of  $D_{50}$  for the 5  
182 different psd A to E. In general,  $\langle R_d \rangle$  increases when  $D_{50}$  increases and the standard deviation  
183 decreases for smaller particles sizes. Thus, the response is more variable for coarser material.  
184 In addition, as  $D_{max}/D_{min}$  increases, we found that  $\langle R_d \rangle$  slightly decreases and that the standard  
185 deviation decreases. Thus, it seems that  $\langle R_d \rangle$  decreases faster as function of  $D_{50}$  than for the  
186 effect of spreading. As the quantity of smaller particles increases, the response given by the  
187 load-penetration curve is more repeatable.

188 The oscillations of the load-penetration curve vary as function of the combination of their  
189 frequencies  $f_k$  and the associated amplitudes  $A_k$ . We can observe on the load-penetration curves  
190 of Fig.10 and 11 than the amplitudes of oscillations decrease and the frequency increases as the  
191 material becomes finer. It is then more difficult to detect the frequency features for finer  
192 materials i.e C or E.

193 In order to quantify the oscillations of the load-penetration curve for each material and in order  
194 to compare them to each other, we defined the coefficient  $Af$  as the average value of the product  
195 of the frequency  $f_k$  and the associated amplitude  $A_k$  detected in the band-pass range  $[f_{trans}, f_{limit}]$ .

$$Af = \frac{\sum_{k=1}^n A_k \times f_k}{n} \quad (5)$$

196 with  $n$  the number of frequencies detected in band-pass range  $[f_{trans}, f_{limit}]$ .

197 Figure 13 presents the coefficient  $A_f$  averaged on 15 impacts for each material  $A$  to  $E$  as function  
198 of  $D_{50}$  and of PSD spreading. We found that  $\langle A_f \rangle$  and its standard deviation decrease as the  
199 average diameter  $D_{50}$  decreases. The coefficient  $\langle A_f \rangle$  was also found to decrease as the  
200 spreading of PSD increases. It means that the oscillations of load-penetration curve, quantified  
201 by a coefficient  $\langle A_f \rangle$ , are dependent on the PSD of the material tested.

## 202 5. Conclusions

203 In this paper, we presented a method to analyze the dynamic penetration test results, based on  
204 the Discrete Fourier Transform. This method was used on results of dynamic penetration test  
205 of Panda modelled in 2D with DEM. The method was applied to the evaluation of the variation  
206 of particle size distribution of a coarse granular material, on and more particularly the influence  
207 of average particle diameter and particle size distribution span. Five different materials were  
208 simulated under dynamic penetration test.

209 The discrete Fourier transform was applied on the load vs. penetration curves so that:

- 210 • the oscillations of the penetration curve can be reconstructed
- 211 • a band-pass range that characterizes the material in terms of particle size distribution  
212 can be identified
- 213 • influence of mean diameter  $D_{50}$  on the both global response and signal oscillations can  
214 be quantified with a scalar called here amplitude coefficient  $\langle A_f \rangle$  calculated from the  
215 frequencies and associated amplitudes in the characteristic band-pass range. This  
216 coefficient captures only the nature of the oscillations and is influenced by particle size  
217 distribution of the material.

218 Concerning the macroscopic response, we observed that

- 219 • average tip resistance decreases when the content of smaller particles increases: when  
220  $D_{50}$  decreases and when the spreading of the particle size distribution increases
- 221 • the DFT applied on signal obtained with finer granular materials shows a distribution  
222 of frequencies and associated amplitude that is more flat, in the characteristic band-pass  
223 range, making it more difficult to detect the characteristic frequency and amplitude of  
224 the oscillations for such materials.

225 The method presented in this paper based on spectral analysis will be useful to extract more  
226 information from the penetrometer test results, in terms of physical properties of the material,  
227 and beyond the classical tip resistance. Further investigations using three-dimensional modeling

228 and experimental validation will have to be performed in order to confirm and extend the  
229 benefits of this method.

- 231 [1] Chaigneau, L.: *Caractérisation des milieux granulaires de surface à l'aide d'un*  
232 *pénétrömètre*. PhD thesis. Clermont-Ferrand: Université Blaise Pascal (2001)  
233
- 234 [2] Breul, P., Benz, M., Gourvès, R., Saussine, G.: Penetration Test Modelling in a Coarse  
235 Granular Medium. In *Powders and Grains 2009: Proceedings of the 6<sup>th</sup> International*  
236 *Conference on Micromechanics of Granular Media*, 1145(1), pp.173-176, AIP Publishing  
237 (2009)  
238
- 239 [3] Benz Navarrete, M.: *Mesures dynamiques lors du battage du pénétromètre Panda 2*. PhD  
240 thesis, Clermont-Ferrand: Université Blaise Pascal (2009)  
241
- 242 [4] Escobar E., Benz Navarrete M., Gourvès R., Haddani Y., Breul P., Chevalier B.: Dynamic  
243 Characterization of the Supporting Layers in Railway Tracks Using the Dynamic Penetrometer  
244 Panda 3®, *Procedia Engineering*, 143, (2016) 1024-1033  
245 <http://dx.doi.org/10.1016/j.proeng.2016.06.099>.  
246
- 247 [5] Benz, M.A., Escobar, E., Gourvès, R., Haddani, Y., Breul, P. Bacconnet, C. Dynamic  
248 measurements of the penetration test - Determination of the tip's dynamic load penetration  
249 curve. *Proc. of the 18th Int. Conf. on the Soil Mech. and Geotech. Eng., Paris*, pp.499-502  
250 (2013)  
251
- 252 [6] Escobar Valencia E.J.: *Mise au point et exploitation d'une nouvelle technique pour la*  
253 *reconnaissance des sols: le PANDA 3*. PhD thesis, Clermont-Ferrand: Université Blaise Pascal  
254 (2015)  
255
- 256 [7] Tran, Q.A., Chevalier, B., Breul, P.: Discrete modeling of penetration tests in constant  
257 velocity and impact conditions. *Computers and Geotechnics*, 71, 12-18 (2016)  
258
- 259 [8] Huang A.B., Ma M.Y.: An analytical study of cone penetration test in granular material.  
260 *Can Geotech J*, 31(1), 91-103. (1994)  
261
- 262 [9] Huang A.B., Hsu H.H.: Advanced calibration chambers for cone penetration testing in  
263 cohesionless soils. In: *ISC-2 Geotech and Geophys Site Characterization*, pp.147-66, Porto,  
264 (2004)  
265
- 266 [10] Calvetti F., Nova R.: Micro–macro relationships from DEM simulated element and in-situ  
267 tests. In: *Proc 5th Int Conf Micromech Granular Media: Powders and Grains 2005*, Stuttgart,  
268 pp.245-250 (2005)  
269
- 270 [11] Jiang M.J., Yu H.-S., Harris D.: Discrete element modeling of deep penetration in granular  
271 soils. *Int J Numer Anal Meth Geomech*, 30(4), 335-61 (2006)  
272
- 273 [12] Jiang MJ, Harris D, Zhu H.: Future continuum models for granular materials in penetration  
274 analyses. *Granular Matter*, 9(1), 97-108. (2007)  
275
- 276 [13] Jiang M, Dai Y, Cui L, Shen Z, Wang X.: Investigating mechanism of inclined CPT in  
277 granular ground using DEM. *Granular Matter*, 16(5), 785-96 (2014)  
278

- 279 [14] Tran Q.A., Chevalier B., Breul P.: A numerical study of the penetration test at constant rod  
280 velocity. In: *Oka, Murakami, Uzuoka, Kimoto, editors. Computer methods methods and recent*  
281 *advances in geomechanics*, pp. 193–8, Kyoto (2015)  
282
- 283 [15] Janda, A., Ooi, J. Y.: DEM modeling of cone penetration and unconfined compression in  
284 cohesive solids. *Powder Technology* (2015). doi: 10.1016/j.powtec.2015.05.034  
285
- 286 [16] Arroyo M., Butlanska J., Gens A., Calvetti F., Jamiolkowski M.: Cone penetration tests in  
287 a virtual calibration chamber. *Géotechnique*, 61(6), 525-31. (2011)  
288
- 289 [17] Butlanska, J., O Sullivan C, Arroyo M., Gens A., Jiang M., Liu F. and Bolton M: Mapping  
290 deformation during CPT in a virtual calibration chamber, in *Proceedings of the International*  
291 *Symposium on Geomechanics and Geotechnics: From Micro to Macro*. Taylor & Francis Group  
292 Eds., pp.559-564 (2011)  
293
- 294 [18] McDowell G.R., Falagush O, Yu H.S.: A particle refinement method for simulating DEM  
295 of cone penetration testing in granular materials. *Geotech Lett*, 2, 141-7 (2012)  
296
- 297 [19] Quezada, J.C., Breul, P., Saussine, G., Radjai, F.: Penetration test in coarse granular  
298 material using Contact Dynamics Method. *Computers and Geotechnics*, 55, 248-253 (2014)  
299
- 300 [20] Ciantia, M.O., Arroyo, M., Butlanska, J., Gens, A.: DEM modelling of cone penetration  
301 tests in a double-porosity crushable granular material. *Computers and Geotechnics*, 73, 109-  
302 127 (2016)  
303
- 304 [21] Cundall P.A., Strack O.D.L.: A discrete numerical model for granular assemblies.  
305 *Géotechnique*, 29(1), 47-65 (1979)  
306
- 307 [22] Combe G. *Mécanique des matériaux granulaires et origines microscopiques de la*  
308 *déformation*. Etudes et Recherches du Laboratoire Central des Ponts et Chaussées. SI8. (2002)  
309
- 310 [23] Roux J.-N., Chevoir F.: Discrete numerical simulation and the mechanical behavior of  
311 granular materials. *Bulletin du Laboratoire des Ponts et Chaussées*, 254,109-138 (2005)  
312
- 313 [24] Tran Q.A.: *Modélisation numérique du comportement des milieux granulaires à partir de*  
314 *signaux pénétrométriques: approche micromécanique par la méthode des éléments discrets*.  
315 PhD thesis , Université Blaise Pascal-Clermont-Ferrand II (2015)  
316  
317

318 Table 1. Parameters of the model.

<i>Parameter</i>	<i>Symbol</i>	<i>Value</i>	<i>Unit</i>
Width box	$L$	0.60	m
Height box	$H$	0.45	m
Particle density	$\rho$	2 700	kg.m <sup>-3</sup>
Normal contact stiffness	$k_n$	1.25 x 10 <sup>8</sup>	N.m <sup>-1</sup>
Tangential contact stiffness	$k_s$	9.375 x 10 <sup>7</sup>	N.m <sup>-1</sup>
Rod friction coefficient	$\mu_{rod}$	0.0	–
Tip friction coefficient	$\mu_{tip}$	0.3	–

319

320 Table 2. Material characteristics used in penetration tests with different particle size  
321 distribution.

Ref	Particle number $N_p$	$\phi_{max}$ [-]	$D_{max}$ [mm]	$D_{50}$ [mm]	$D_{max}/D_{min}$ [-]	Type
A	10 000	0.844	7.02	5.80	2	I;II
B	40 000	0.843	3.51	2.91	2	I
C	160 000	0.843	1.76	1.45	2	I
D	30 000	0.856	7.02	3.98	5	II
E	97 831	0.869	7.02	2.61	10	II

322  
323

324 List of figure captions

325 Figure 1. Experimental result of dynamic penetration test [12]

326 Figure 2. Example of experimental load-penetration curve obtained in a dynamic penetration test for  
327 one impact [3]

328 Figure 3. View of the numerical model of the tip and of the container for the penetration test in  
329 dynamic conditions (Tran et al., 2015)

330 Figure 4. Particle size distribution (a) for different average particle diameters (materials A, B and C)  
331 and (b) for different particle size distribution shapes (materials A, D and E)

332 Figure 5. Example of load-penetration curves obtained in a dynamic cone penetration test for 3  
333 impacts in material A

334 Figure 6. Example of the amplitude spectrum of one impact of the material A with different numbers  
335 of  $N$ -points DFT

336 Figure 7. Example of the amplitude spectrum of five impacts for two materials A and C

337 Figure 8. Relative error for one impact of the material A

338 Figure 9. (*Left*) Comparison of the raw load-penetration curve for the material A with signal  
339 reconstructed with frequency ranges  $[0, f_{trans}]$  and  $[0, f_{limited}]$ . (*Right*) Signal reconstructed with  
340 frequency range  $[f_{trans}, f_{limited}]$  showing the major oscillations of load-penetration curve

341 Figure 10. Tip force as a function of penetration distance for 5 successive dynamic penetration tests  
342 for materials A, B and C

343 Figure 11. Tip force as a function of penetration distance for 5 successive dynamic penetration tests  
344 for materials A, D and E

345 Figure 12. (*Left*)  $\langle R_d \rangle$  as function of  $D_{50}$  with five PSD A to E. (*Right*)  $\langle R_d \rangle$  as function of PSD shape  
346 for three materials A, D and E (height of vertical bars is twice the standard deviation of  $R_d$ )

347 Figure 13. (*Left*)  $\langle Af \rangle$  as fonction of  $D_{50}$  for five particle size distributions A to E. (*Right*)  $\langle Af \rangle$  as  
348 function of psd shape for three particle size distributions A, D and E (height of vertical bars represent  
349 twice the standard deviation of  $\langle Af \rangle$ )

350

Figure 1. Experimental result of dynamic penetration test [12]

Figure 2. Example of experimental load-penetration curve obtained in a dynamic penetration test for one impact [3]

Figure 3. View of the numerical model of the tip and of the container for the penetration test in dynamic conditions (Tran et al., 2015)

Figure 4. Particle size distribution (a) for different average particle diameters (materials A, B and C) and (b) for different particle size distribution shapes (materials A, D and E)

Figure 5. Example of load-penetration curves obtained in a dynamic cone penetration test for 3 impacts in material A

Figure 6. Example of the amplitude spectrum of one impact of the material A with different numbers of  $N$ -points DFT

Figure 7. Example of the amplitude spectrum of five impacts for two materials A and C

Figure 8. Relative error for one impact of the material A

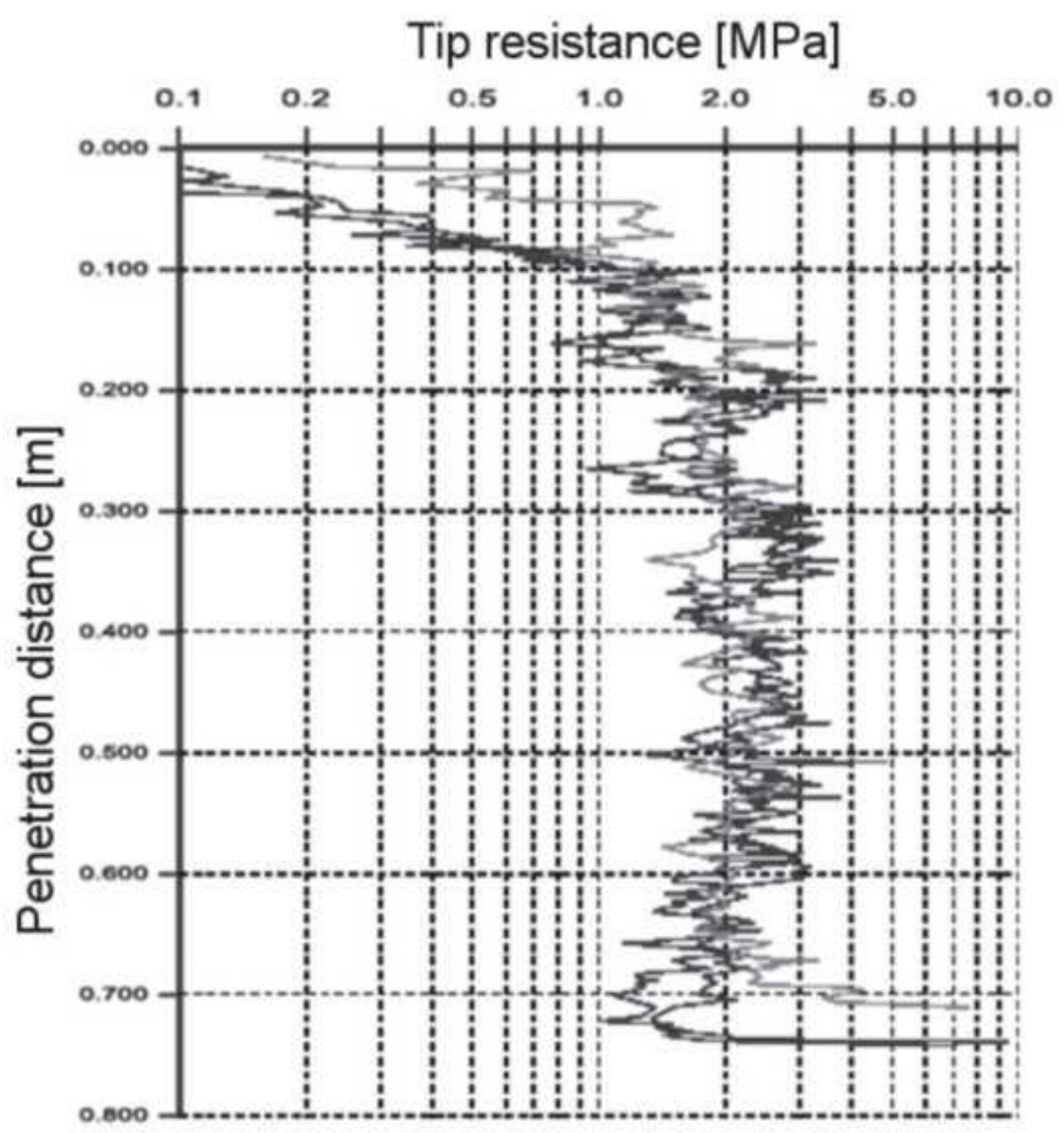
Figure 9. (*Left*) Comparison of the raw load-penetration curve for the material A with signal reconstructed with frequency ranges  $[0, f_{trans}]$  and  $[0, f_{limited}]$ . (*Right*) Signal reconstructed with frequency range  $[f_{trans}, f_{limited}]$  showing the major oscillations of load-penetration curve

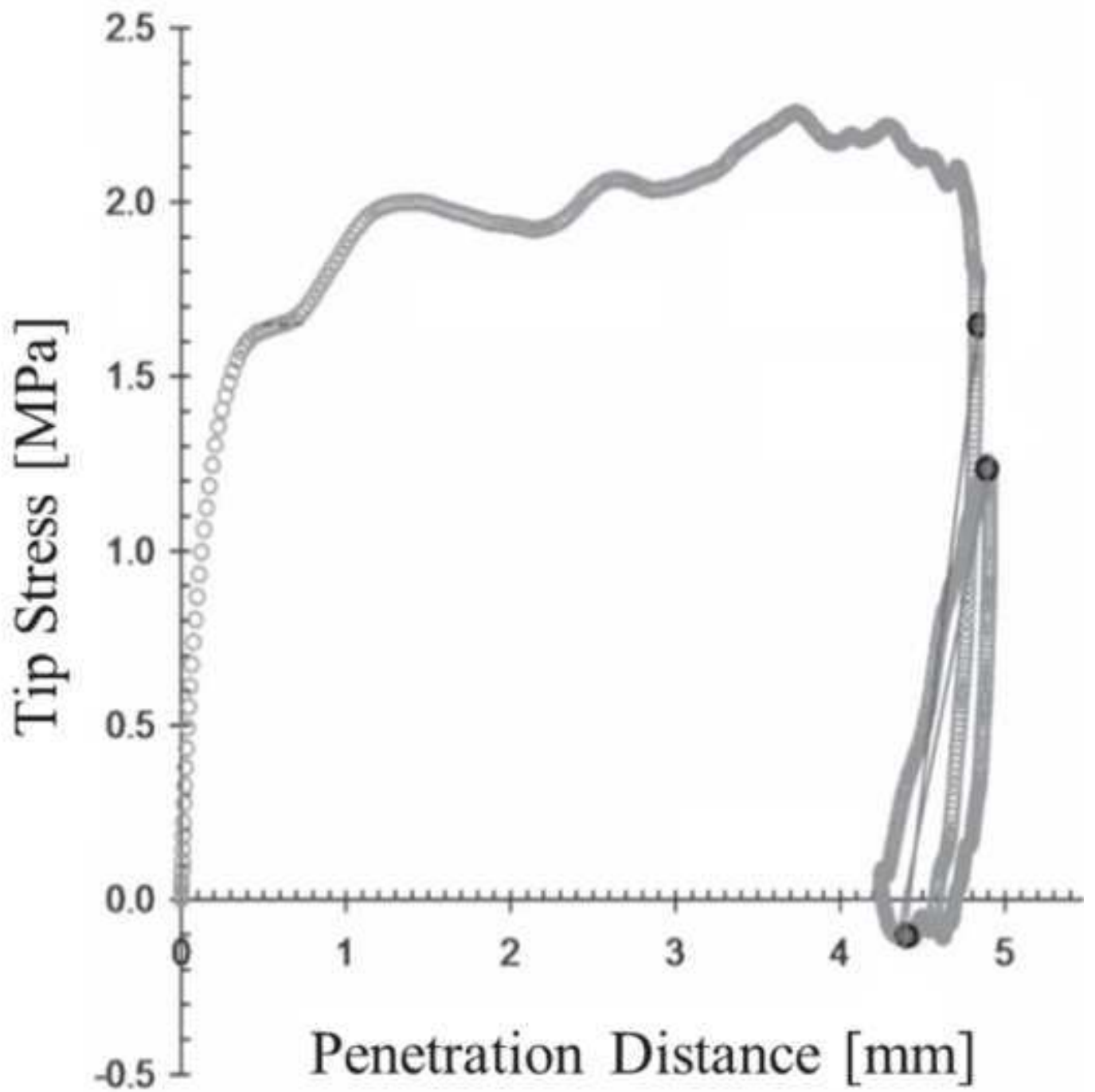
Figure 10. Tip force as a function of penetration distance for 5 successive dynamic penetration tests for materials A, B and C

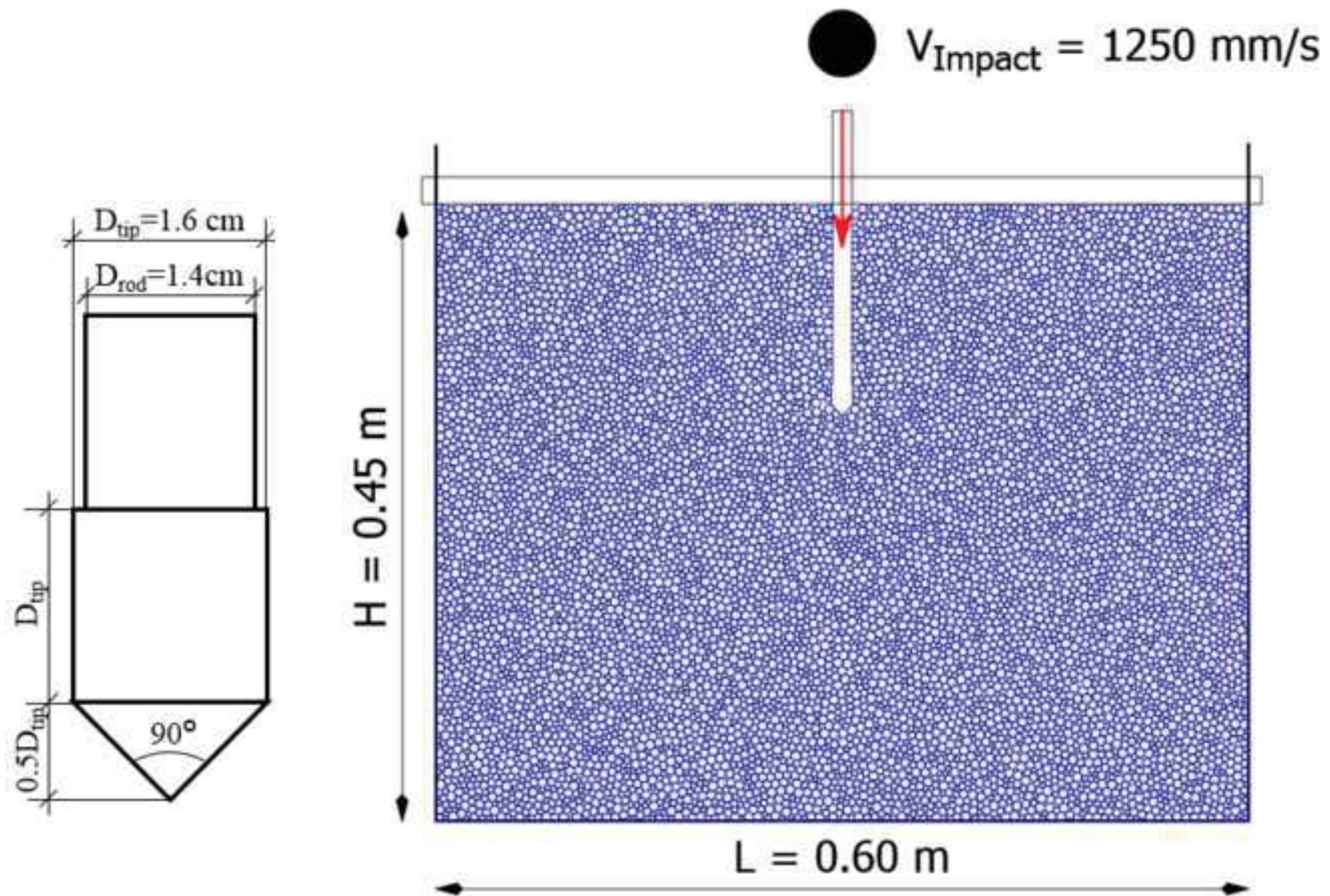
Figure 11. Tip force as a function of penetration distance for 5 successive dynamic penetration tests for materials A, D and E

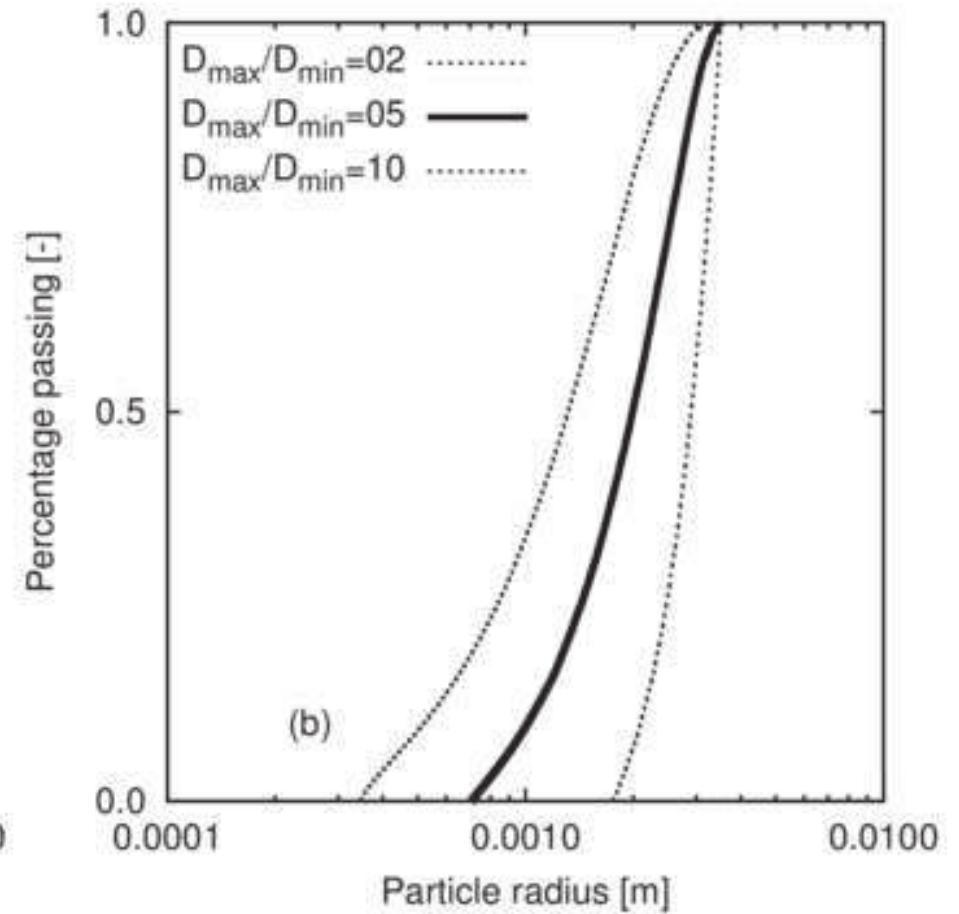
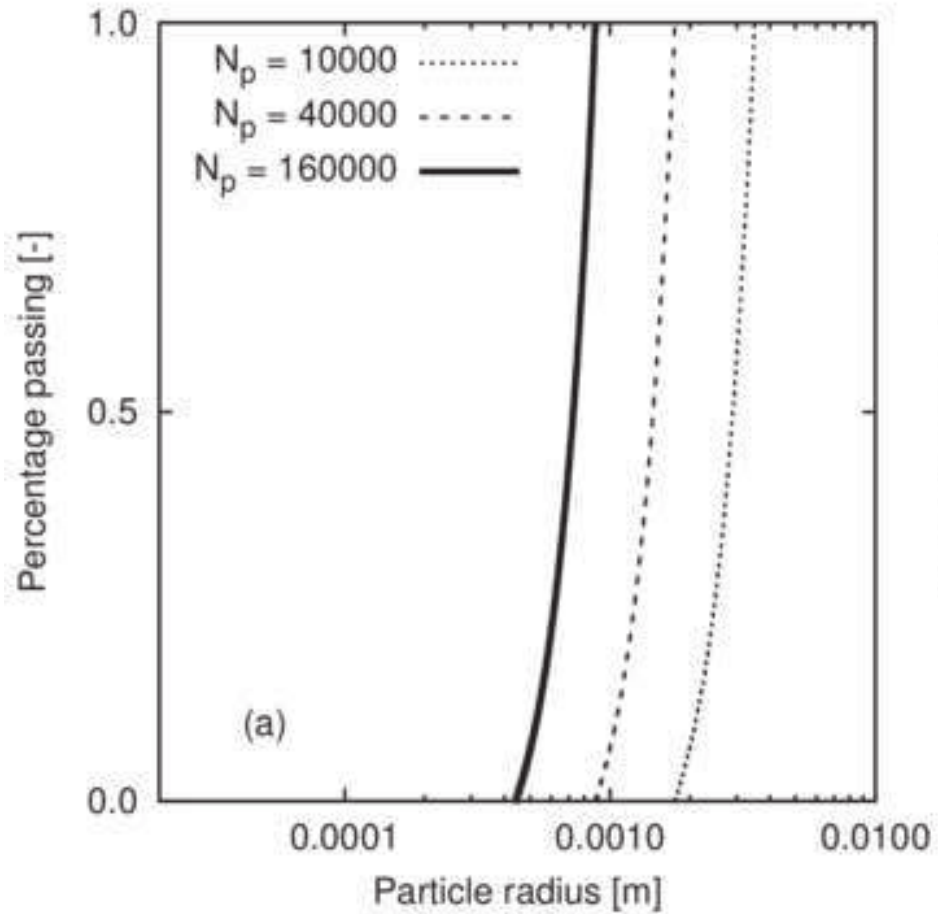
Figure 12. (*Left*)  $\langle R_d \rangle$  as function of  $D_{50}$  with five PSD A to E. (*Right*)  $\langle R_d \rangle$  as function of PSD shape for three materials A, D and E (height of vertical bars is twice the standard deviation of  $R_d$ )

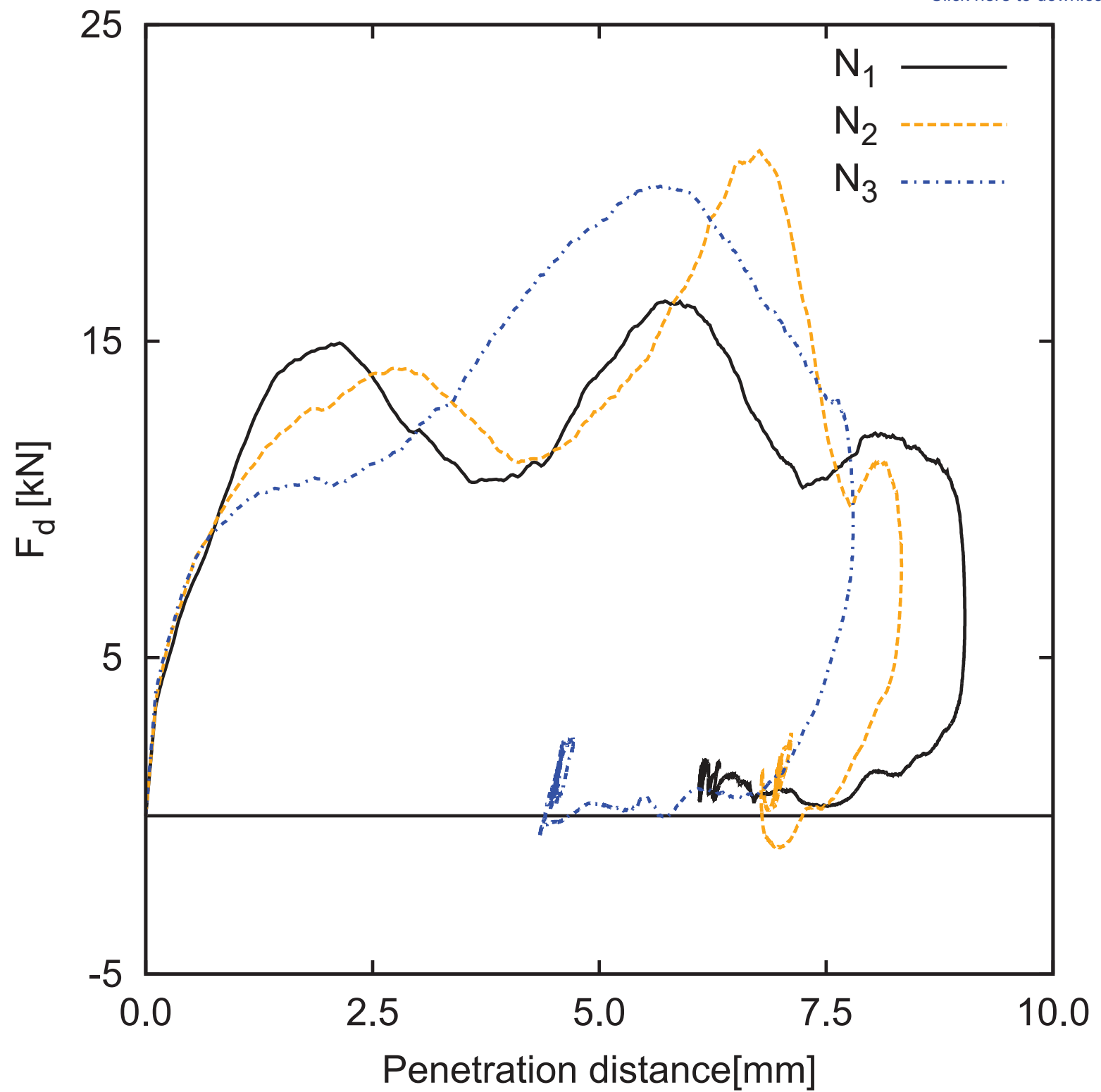
Figure 13. (*Left*)  $\langle Af \rangle$  as fonction of  $D_{50}$  for five particle size distributions A to E. (*Right*)  $\langle Af \rangle$  as function of psd shape for three particle size distributions A, D and E (height of vertical bars represent twice the standard deviation of  $\langle Af \rangle$ )

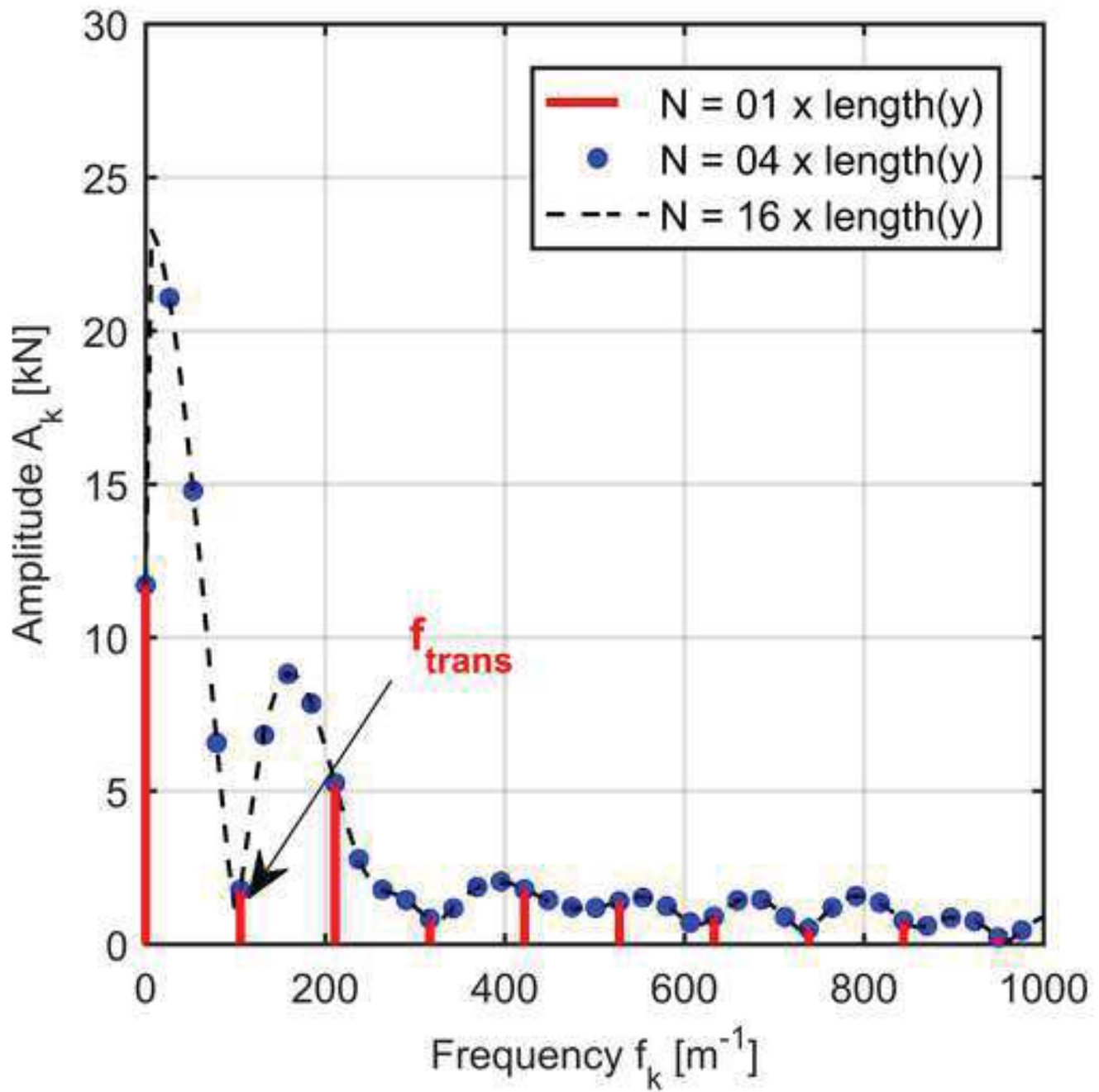


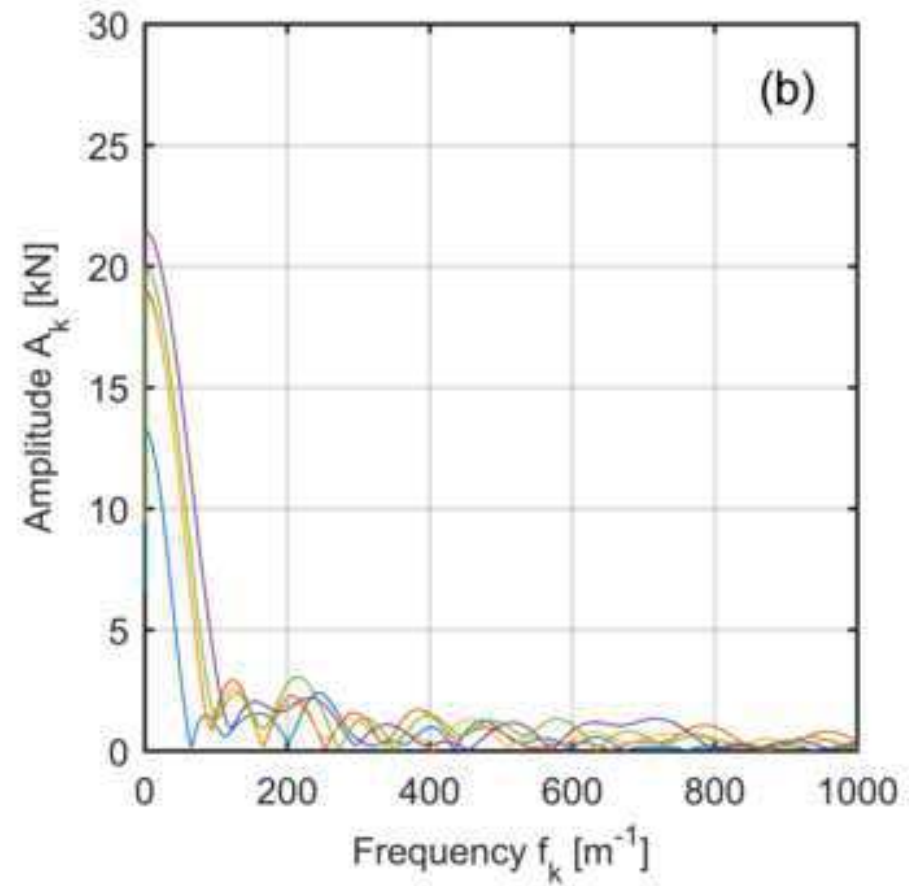
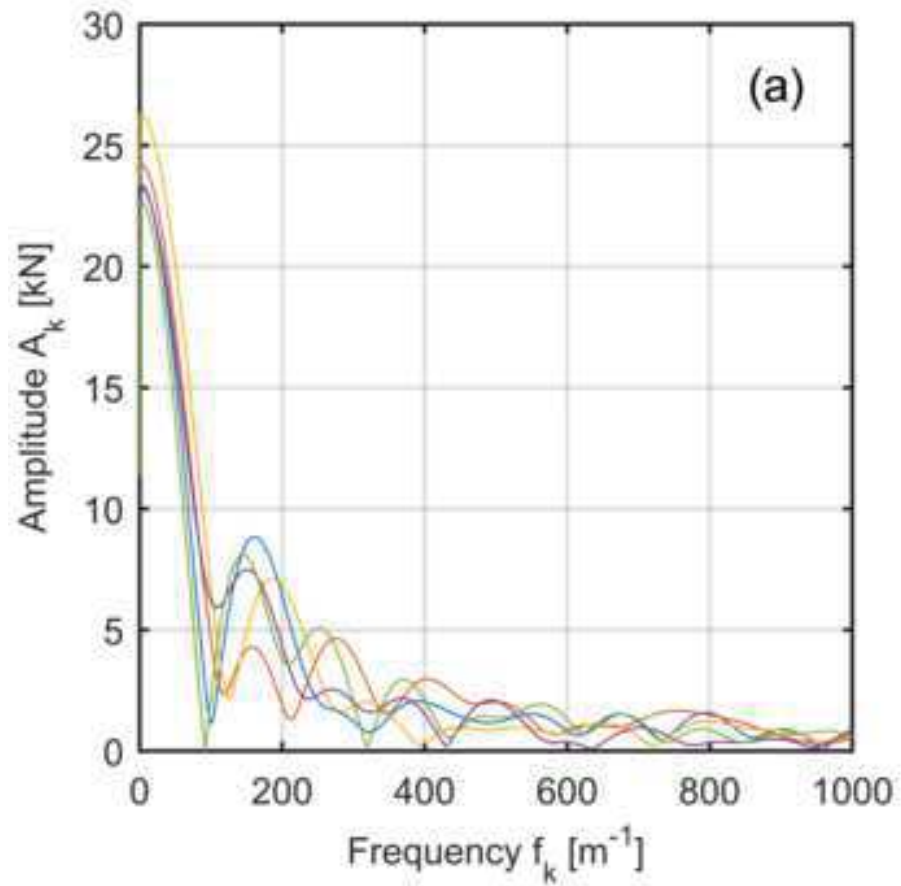


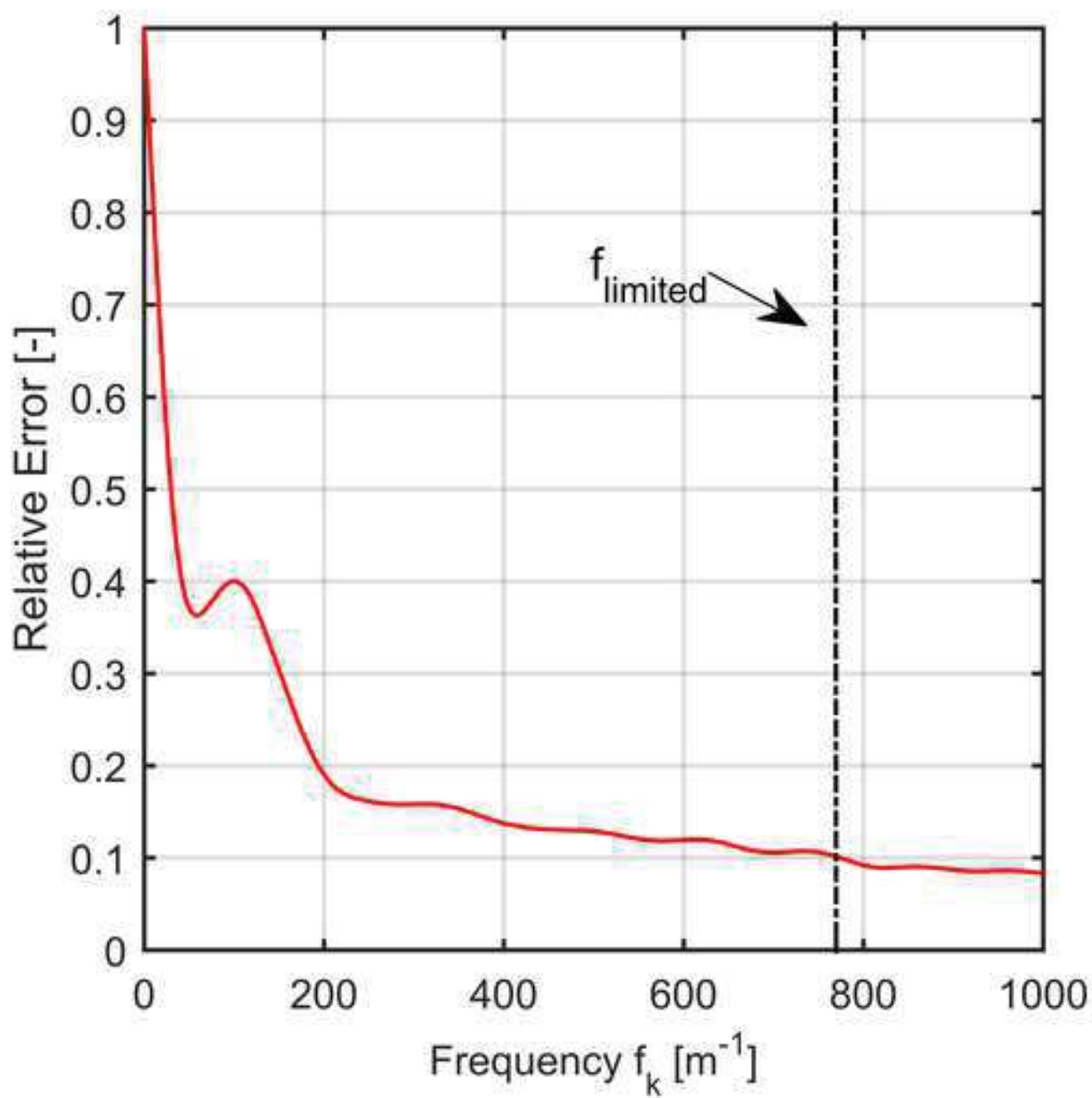












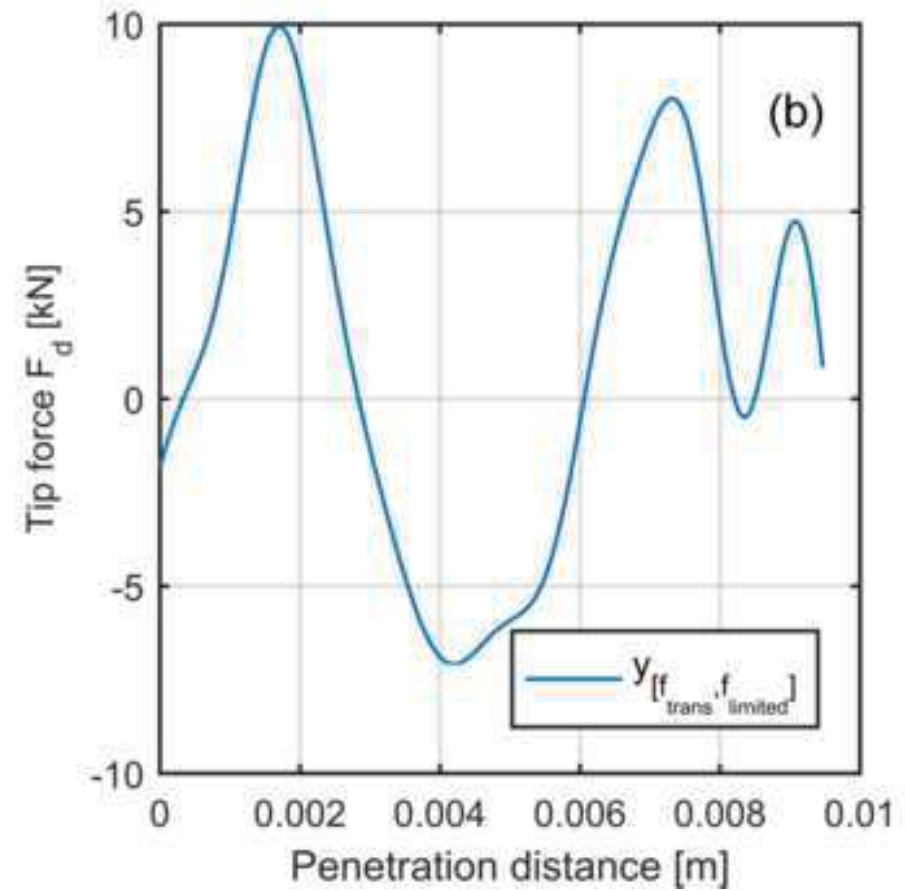
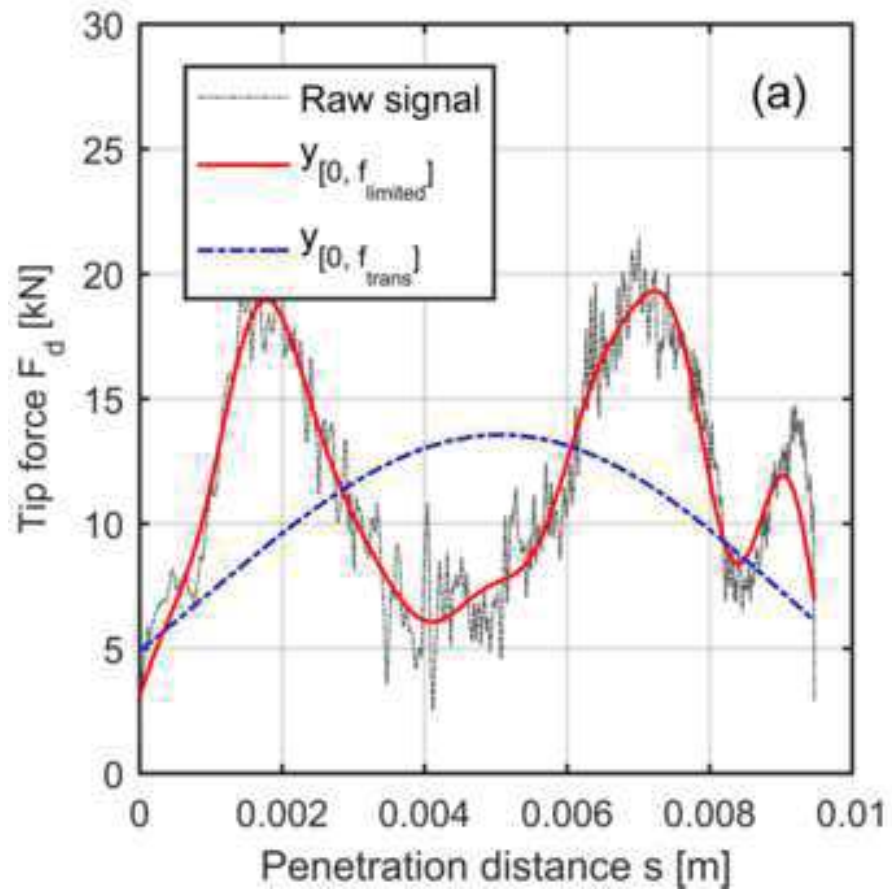


Fig.10

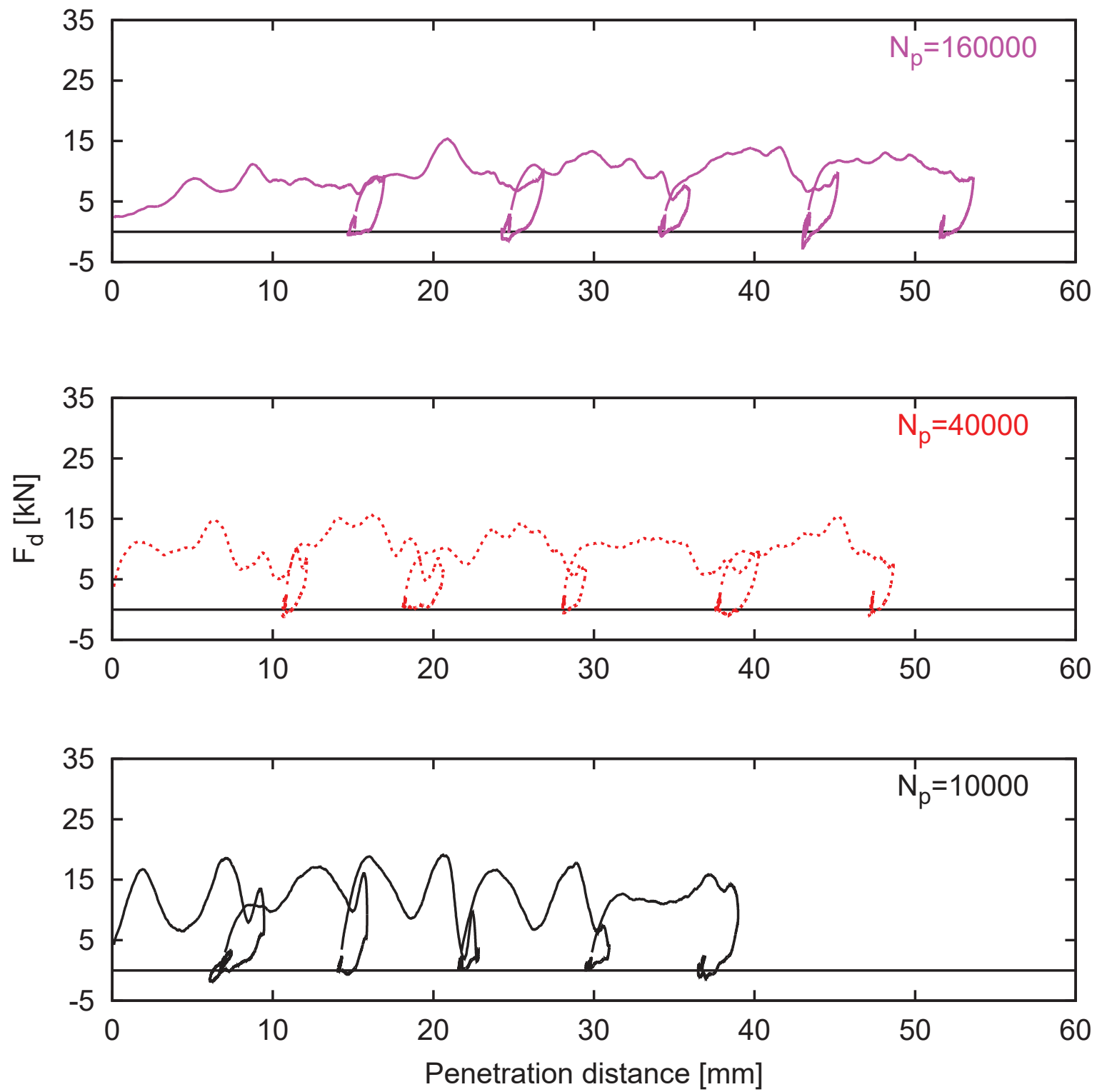


Fig.11

